European Radiology (2019) 29:2669–2676
https://doi.org/10.1007/s00330-018-5892-2

NEURO

Wavelet-based reconstruction of dynamic susceptibility MR-perfusion: a new method to visualize hypervascular brain tumors

Thomas Huber[1] · Lukas Rotkopf[1,2] · Benedikt Wiestler[2] · Wolfgang G. Kunz[1] · Stefanie Bette[2] · Jens Gempt[3] · Christine Preibisch[2] · Jens Ricke[1] · Claus Zimmer[2] · Jan S. Kirschke[2] · Wieland H. Sommer[1] · Kolja M. Thierfelder[1,4]

Received: 11 August 2018 / Revised: 16 October 2018 / Accepted: 14 November 2018 / Published online: 14 December 2018

Abstract

Objectives Parameter maps based on wavelet-transform post-processing of dynamic perfusion data offer an innovative way of visualizing blood vessels in a fully automated, user-independent way. The aims of this study were (i) a proof of concept regarding wavelet-based analysis of dynamic susceptibility contrast (DSC) MRI data and (ii) to demonstrate advantages of wavelet-based measures compared to standard cerebral blood volume (CBV) maps in patients with the initial diagnosis of glioblastoma (GBM).

Methods Consecutive 3-T DSC MRI datasets of 46 subjects with GBM (mean age 63.0 ± 13.1 years, 28 m) were retrospectively included in this feasibility study. Vessel-specific wavelet magnetic resonance perfusion (wavelet-MRP) maps were calculated using the wavelet transform (Paul wavelet, order 1) of each voxel time course. Five different aspects of image quality and tumor delineation were each qualitatively rated on a 5-point Likert scale. Quantitative analysis included image contrast and contrast-to-noise ratio.

Results Vessel-specific wavelet-MRP maps could be calculated within a mean time of 2:27 min. Wavelet-MRP achieved higher scores compared to CBV in all qualitative ratings: tumor depiction (4.02 vs. 2.33), contrast enhancement (3.93 vs. 2.23), central necrosis (3.86 vs. 2.40), morphologic correlation (3.87 vs. 2.24), and overall impression (4.00 vs. 2.41); all $p < .001$. Quantitative image analysis showed a better image contrast and higher contrast-to-noise ratios for wavelet-MRP compared to conventional perfusion maps (all $p < .001$).

Conclusions wavelet-MRP is a fast and fully automated post-processing technique that yields reproducible perfusion maps with a clearer vascular depiction of GBM compared to standard CBV maps.

Key Points

- *Wavelet-MRP offers high-contrast perfusion maps with a clear delineation of focal perfusion alterations.*
- *Both image contrast and visual image quality were beneficial for wavelet-MRP compared to standard perfusion maps like CBV.*
- *Wavelet-MRP can be automatically calculated from existing dynamic susceptibility contrast (DSC) perfusion data.*

Keywords Brain neoplasms · Cerebral blood volume · Glioblastoma · Perfusion imaging · Wavelet analysis

Abbreviations

AIF	Arterial input function
CBF	Cerebral blood flow
CBV	Cerebral blood volume
CNR	Contrast-to-noise ratio
DCE	Dynamic contrast enhanced
DSC	Dynamic susceptibility contrast
FLAIR	Fluid-attenuated inversion recovery
GBM	Glioblastoma
ICC	Intra-class correlation
MPRAGE	Magnetization prepared rapid gradient echo
MTT	Mean transit time
PRESTO	Principles of echo-shifting with a train of observations sequence
PWI	Perfusion-weighted imaging

Electronic supplementary material The online version of this article (https://doi.org/10.1007/s00330-018-5892-2) contains supplementary material, which is available to authorized users.

✉ Thomas Huber
thomas.huber@med.uni-muenchen.de

[1] Department of Radiology, University Hospital, LMU Munich, Marchioninistr. 15, 81377 Munich, Germany

[2] Department of Neuroradiology, Klinikum rechts der Isar, Technical University of Munich, Ismaninger Str. 22, 81675 Munich, Germany

[3] Department of Neurosurgery, Klinikum rechts der Isar, Technical University of Munich, Ismaninger Str. 22, 81675 Munich, Germany

[4] Institute of Diagnostic and Interventional Radiology, University Medicine Rostock, Schillingallee 35, 18057 Rostock, Germany

TTP	Time to peak
wavelet-MRP	Wavelet magnetic resonance perfusion

Introduction

Perfusion-weighted imaging (PWI) is a standard technique in magnetic resonance imaging (MRI) to assess vascularization of brain tumors. In neuro-oncology, T2*-weighted dynamic susceptibility contrast (DSC) PWI is used at many specialized centers to visualize tumor vascularization in glioblastoma (GBM). For this purpose, relative (r) cerebral blood volume (CBV) has been proven to be one of the most useful PWI parameters [1, 2].

rCBV correlates well with glioma malignancy [3, 4] and especially GBM is characterized by hypervascular tumor tissue which can be visualized in CBV maps [5, 6]. PWI is further often applied as a tool for tumor monitoring, to detect recurrent disease, and to differentiate between tumor recurrence and radiation necrosis [7, 8]. Further, it has been shown that rCBV can be used as a parameter for therapy response assessment [9, 10].

Although rCBV is commonly used in the diagnostic work-up and follow-up of GBM patients, there are a number of drawbacks limiting its diagnostic impact and reproducibility. For instance, different algorithms for deconvolution are used depending on the post-processing software [11]. Further, standard perfusion images are often difficult to read as tumor tissue may exhibit a relatively low contrast compared to normal gray and white matter [12]. Therefore, focal rCBV alterations in follow-up MRI of GBM might be missed even though they could be a sign of a tumor recurrence [7]. Thus, high-contrast perfusion maps with a clearer delineation of focal perfusion alterations would be highly beneficial.

A new wavelet-transform post-processing technique has recently been applied to dynamic computed tomography (CT) perfusion data to obtain detailed angiographic images [13, 14] with a higher vascular contrast while suppressing non-contrast–enhancing structures such as bone [13]. Wavelet-transform post-processing might also turn out to be beneficial for evaluation of MR-based PWI. This would potentially mitigate some of the abovementioned disadvantages of CBV calculations.

The aims of this study were a proof of concept using a wavelet-based analysis of DSC PWI and to demonstrate potential advantages of the wavelet technique compared to rCBV maps in GBM.

Methods

Patient population

Imaging data were obtained from a cohort of patients with the initial diagnosis of glioblastoma (GBM) who were examined between November 2009 and August 2016. Selected patients needed to fulfill the following inclusion criteria:

1. Initial diagnosis of GBM as histologically confirmed in resected specimen by the local Department of Neuropathology.
2. Preoperative MRI including at least T2-weighted fluid-attenuated-inversion-recovery (FLAIR) sequences and contrast-enhanced T1-weighted sequences.
3. Availability of DSC imaging time series.

From 49 consecutive patients, three patients had to be excluded due to insufficient contrast agent application ($n = 2$) and due to invalid settings in the DSC perfusion sequence ($n = 1$), respectively. General image quality was evaluated by one reader (LR). The final cohort consisted of 46 patients (28 male, 63.0 years ± 13.1) who were selected retrospectively in this single-center study at a maximum care university hospital.

Acquisition protocol

All patients underwent preoperative MRI on a 3-Tesla (T) Achieva MR scanner (Philips Medical Systems). MR protocols included a high-resolution T2-weighted fluid-attenuated inversion recovery (FLAIR) sequence and a T1-weighted magnetization prepared rapid gradient echo (MPRAGE) sequence (spatial resolution 1 × 1 × 1 mm; TR/TE 9/4 ms; inversion time TI 900 ms). DSC MRI was performed using dynamic acquisitions of either a principles of echo-shifting with a train of observations (PRESTO) sequence (18 patients) [15] or single-shot gradient-echo EPI protocols (28 patients). Adapted to the patients' weights, 15 to 20 ml of either Magnograf® (MaRoTrast) or Dotarem® (Guerbet) was administered at a flow rate of 4 ml per second.

Image post-processing

Wavelet-MRP DICOM images were imported to a customized Python 3.5 script (Python Software Foundation). A Python implementation of the continuous wavelet transform was used [16]. Rigid-body motion correction was performed using SimpleElastix (https://simpleelastix.github.io) [17]. After correction, parameter values were calculated for each voxel by applying a continuous wavelet transformation over the time signal curve using the Paul wavelet of order $m = 1$ [13].

Calculation of stationary wavelet power coefficients The continuous wavelet transform of the DSC signal time curve $x(t)$, in this case the untruncated signal curve, is defined by:

$$w(u,s) = \int_{-\infty}^{\infty} x(t)\ \psi_0{}^{*}\left(\frac{t-u}{s}\right)\ dt$$

with the complex conjugate of the *mother wavelet* $\psi_0{}^*\left(\frac{t-u}{s}\right)$, time t, and scaling parameter s, corresponding to the inverse of the frequency resolution. For the Paul wavelet, the mother wavelet of order m is:

$$\psi_0(t) = \frac{2^m\, i^m\, m!}{\sqrt{(2m)!\pi}}(1-i\,t)^{-(1+m)}$$

The maximum power coefficient is then given by the maximum of the squared coefficient matrix over all scales.

PWI processing Processing of DSC data for relative CBV, cerebral blood flow (CBF), mean transit time (MTT), and time to peak (TTP) was based on integration of the leakage-corrected tissue residue function using an automatically determined AIF (in-house developed scripting suite based on MATLAB R2017a (Mathworks) and SPM12 (http://www.fil.ion.ucl.ac.uk/spm/) as previously reported [18]. Fully leakage-corrected relative standard perfusion sets were successfully obtained for all cases.

Quantitative evaluation: Weber contrast and contrast-to-noise ratio

For a quantitative comparison between the two different post-processing methods, hyperintense tumor-related regions were manually segmented (TH, 4 years of neuroradiological experience) on co-registered contrast-enhanced MPRAGE datasets in ITK-SNAP 3.6.0 (http://www.itksnap.org) [19]. Necrotic tumor regions were removed using a signal threshold on the T1-weighted MPRAGE (Fig. 1). White matter segmentation was done using standard SPM12 algorithms (http://www.fil.ion.ucl.ac.uk/spm/).

Weber image contrast (C) was defined as the differences between the absolute wavelet-MRP or standard PWI parameter (CBV, CBF, MTT, TTP) values in the segmented tumor region and the respective mean values in subcortical white matter, divided by their mean white matter values:

$$C = \frac{I_{tumor} - I_{white\ matter}}{I_{white\ matter}}$$

The contrast-to-noise ratio (CNR) was calculated for wavelet-MRP and conventional PWI parameters by subtracting the subcortical white matter intensity from the signal intensity of the segmented tumor and dividing the difference by the background noise.

$$CNR = \frac{\text{signal difference}}{\text{noise}} = \frac{I_{tumor} - I_{white\ matter}}{\sigma_{tumor+white\ matter}}$$

Qualitative evaluation

Three experienced raters with 6 (KMT), 4 (TH), and 3 (WGK) years of neuroradiological experience evaluated five different aspects of image quality for wavelet-MRP and CBV maps on 5-point Likert scales (1, "non-diagnostic"; 2, "poor"; 3, "fair"; 4, "good"; 5, "excellent"):

- Suppression of background: delineation of tumor against surrounding tissues.
- Definition of contrast enhancement: details of contrast-enhancing tumor structures
- Definition of central necrosis: delineation of the central tumor necrosis
- General morphologic correlation: similarity of morphology to T1w images.
- Overall impression: including clarity, image contrast and depiction of tumor details.

Wavelet-MRP and rCBV maps were presented to the raters for each case together with a contrast-enhanced T1-weighted MPRAGE image using ITK-SNAP and the built-in "auto-contrast" function [19]. Intra-class correlation (ICC) was used to determine consistency among different raters [20, 21].

Statistics and software

Illustrations were compiled using GIMP 2.8.14 (www.gimp.org) and ITK-SNAP 3.6.0. Statistical analyses were performed with IBM SPSS 23.0 (IBM). Differences in contrast, CNR, and qualitative parameters were assessed by paired Wilcoxon signed rank test. Two-sided p values less than .05 were considered significant.

Results

Wavelet-MRP parameter maps were successfully calculated in all 46 subjects. Mean time for wavelet-MRP calculation was 2:27 min per dataset and 18:12 min for the entire dataset including CBV, CBF, MTT, and TTP. All MRI images and calculated maps showed good image quality and no major artifacts.

Quantitative evaluation Image contrast and CNR for wavelet-MRP were significantly higher compared to the conventional DSC perfusion maps for both the whole cohort and the subgroup with an EPI or a PRESTO scan protocol (all $p < .001$, see Table 1, Fig. 2, and Suppl. Tab. 1). The wavelet-MRP signal of the tumor and the image contrast were significantly higher for the EPI protocol (wavelet-MRP signal 1.6E+07 vs. 0.9E+07, $p = .010$; image contrast 8.2 vs. 6.6, $p = .041$); however, there was no significant difference for the wavelet-MRP signal of the white matter, the CNR, or CBV parameters. For

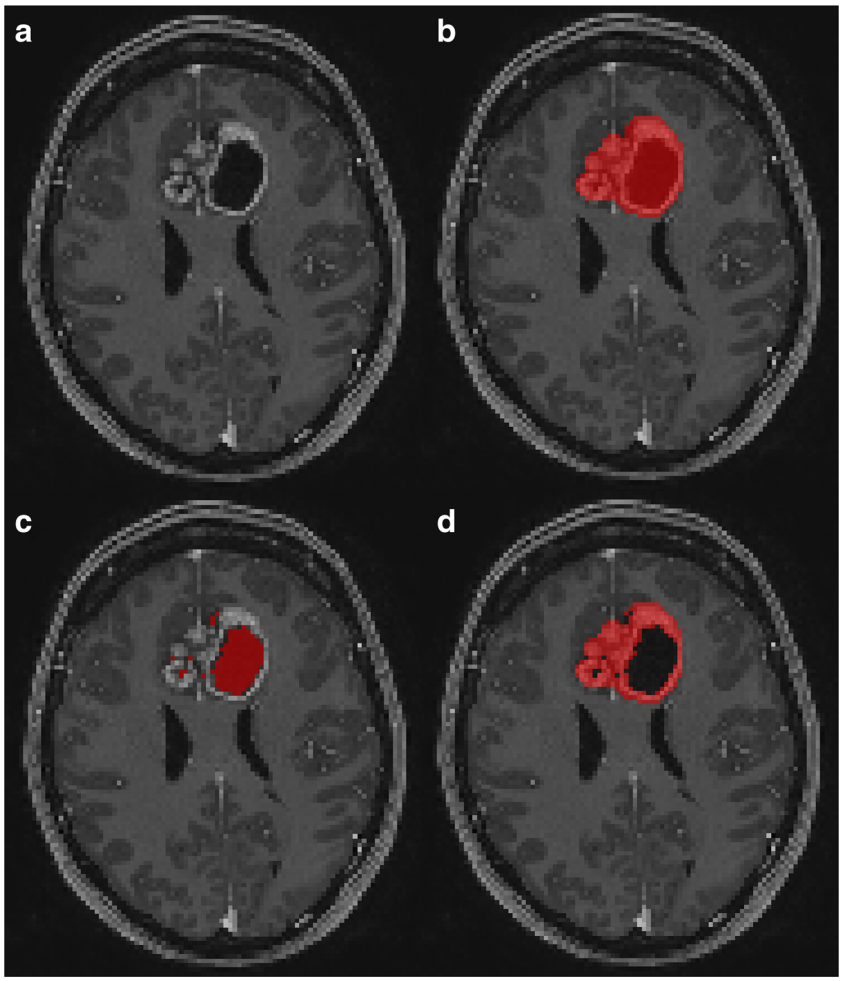

Fig. 1 Illustration of contrast-enhancing tumor segmentation for quantitative image analysis. Contrast-enhanced T1-weighted MPRAGE image showing a butterfly glioblastoma (**a**), whole tumor segmentation (**b**), segmentation of central necrosis (**c**), and contrast-enhancing tumor, defined as the subtraction between whole tumor segmentation and central necrosis (**d**)

the conventional DSC perfusion maps, CBV had the highest image contrast and the best CNR compared to CBF ($p = .122$ and $p < .001$), MTT ($p < .001$ and $p < .001$), and TTP ($p < .001$ and $p < .001$).

Qualitative rating CBV maps had the best image contrast and CNR among the conventional DSC perfusion maps. Therefore, CBV maps and wavelet-MRP parameter maps were qualitatively compared. The category "definition of central necrosis" could only be rated in 45/46 cases due to the absence of a central necrosis in one case. Consistency among the three different expert readers was high. ICC values were as follows: .914 (CI .878–.940) for "suppression of background," .907 (CI .869–.936) for "general morphologic correlation," .906 (CI .867–.935) for "definition of contrast enhancement," .877 (CI .826–.915) for "definition of central necrosis," and .937

Table 1 Results of quantitative image evaluation. Median values and interquartile range (IQR) for wavelet-MRP (wave), CBV, CBF, MTT, and TTP for the contrast-enhancing part of the glioblastoma (CE GBM) and the white matter are shown (wave [unit free], CBV [ml/100 g], CBF [ml/100 g/min], MTT [s], TTP [s]). Image contrast and contrast-to-noise ratio are displayed for wavelet-MRP and compared to the conventional DSC perfusion maps using Wilcoxon test. The results were calculated for the whole cohort (all)

		CE GBM		White matter		Image contrast			Contrast-to-noise ratio		
		Median	IQR	Median	IQR	Median	IQR	Wilcoxon	Median	IQR	Wilcoxon
All ($n = 46$)	Wave	1.3E+07	0.6–2.4E+07	1.5E+06	0.9–3.4E+06	6.8	5.3–9.8		3.5	2.4–5.0	
	CBV	15.5	13.1–19.3	6.8	5.2–7.8	2.7	1.9–3.0	$p < .001$*	1.8	1.2–2.3	$p < .001$*
	CBF	221.1	164.1–284.0	92.6	69.9–122.1	2.5	1.9–3.0	$p < .001$*	1.5	0.9–2.1	$p < .001$*
	MTT	3.4	2.2–4.5	2.5	1.9–3.3	1.3	1.0–1.6	$p < .001$*	0.3	0.1–0.7	$p < .001$*
	TTP	7.3	6.6–8.2	7.4	6.6–7.9	1.0	0.9–1.1	$p < .001$*	0.0	− 0.2 to 0.2	$p < .001$*

P-values less than .05 are marked with an asterisk to indicate significance

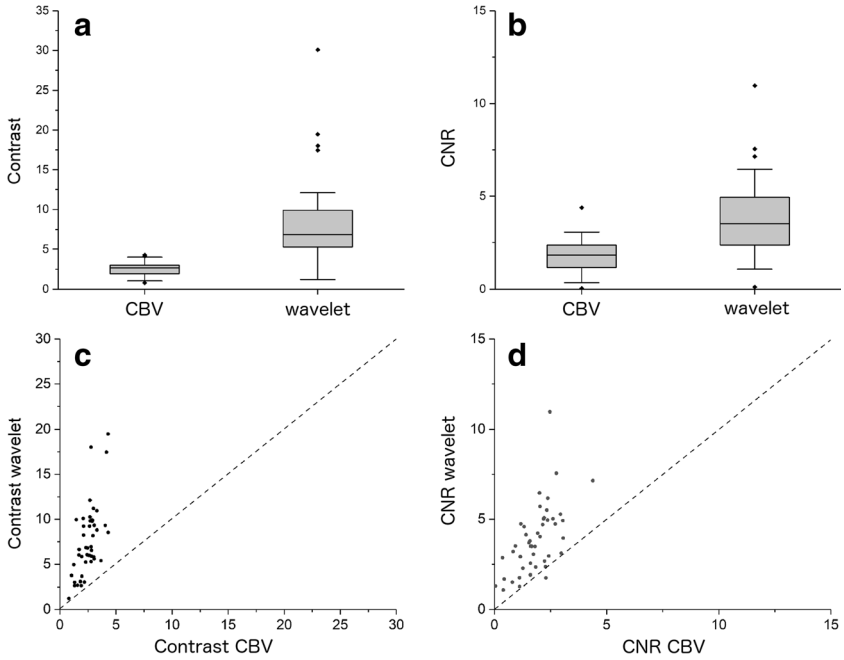

Fig. 2 Box plots of Weber contrast (**a**) and contrast-to-noise ratios (CNR) (**b**) are shown for rCBV and wavelet-MRP for the whole cohort. Scatter diagrams of Weber contrast (**c**) and contrast-to-noise ratios (CNR) illustrate that both parameters were superior for wavelet-MRP than for rCBV maps

(CI .912–.957) for "overall impression." Overall ICC for all qualitative ratings was .908 (CI .892–.922) indicating an excellent inter-rater agreement [21]. Wavelet-MRP obtained significantly higher ratings compared to conventional rCBV maps in all five quality rating categories (Table 2). Maps of wavelet-MRP show a stronger suppression of the background, rendering the GBM tumor border more circumscribed against the adjacent tissue (Fig. 3). Further, necrotic areas (if present) as well as contrast-enhancing tumor parts are depicted in a higher level of detail on maps of wavelet-MRP compared to rCBV (Fig. 4). Of note, there were generally no altered wavelet-MRP parameters in the non-enhancing part of the tumor.

Discussion

Transferring the concept of wavelet-transform post-processing to MRI, we could show that (i) calculation of wavelet-MRP parameter maps is feasible and can be generated within a few minutes; (ii) wavelet-MRP is superior compared to standard rCBV maps in different aspects of image quality; (iii) image contrast and CNR are higher for wavelet-MRP compared to conventional PWI maps. To the best of our knowledge, this is the first study to demonstrate the feasibility of visualization of tumor tissue using wavelet-MRP post-processing.

Reliable post-processing algorithms are essential for obtaining reproducible PWI results. Yet, CBV calculation is often not standardized and shows inter-software variability [22, 23]. Bias is frequently introduced by incorrect selection of the AIF or inaccurate identification of the bolus entry and exit time points [24]. A major advantage of the proposed wavelet-MRP is that it does not require an AIF since the "ideal bolus curve" is modeled by the algorithm itself.

Both qualitative and quantitative results of our study emphasize the power of the wavelet approach in visualizing hypervascular tumors in neuroradiological imaging. Especially that the high conspicuity of tumor compared to background structures was a key feature, enabling a quick and reliable assessment of tumor vascularity. Further, particularly the contrast-enhancing part of the hypervascular tumors was more salient in wavelet-MRP compared to standard rCBV maps. Information on "vascular hotspots" is for example needed for an accurate biopsy

Table 2 Results of qualitative image rating for all raters. Numbers of ratings (*n*), mean scores, and standard deviation (SD) for visual rating on 5-point Likert scales are shown for rCBV and wavelet-MRP. Z-values and *p* scores are shown for Wilcoxon signed-rank test

	CBV		Wavelet-MRP		Wilcoxon	
	Mean	SD	Mean	SD	Z-value	*p*
General morphologic correlation ($n = 46$)	2.24	0.77	3.87	0.83	− 5.78	< .001*
Definition of contrast enhancement ($n = 46$)	2.23	0.74	3.93	0.75	− 5.91	< .001*
Definition of central necrosis ($n = 45$)	2.40	0.86	3.86	0.81	− 5.85	< .001*
Suppression of background ($n = 46$)	2.33	0.72	4.02	0.70	− 5.90	< .001*
Overall impression ($n = 46$)	2.41	0.60	4.00	0.70	− 13.09	< .001*

P-values of less than .05 are marked with asterisk to indicate significance

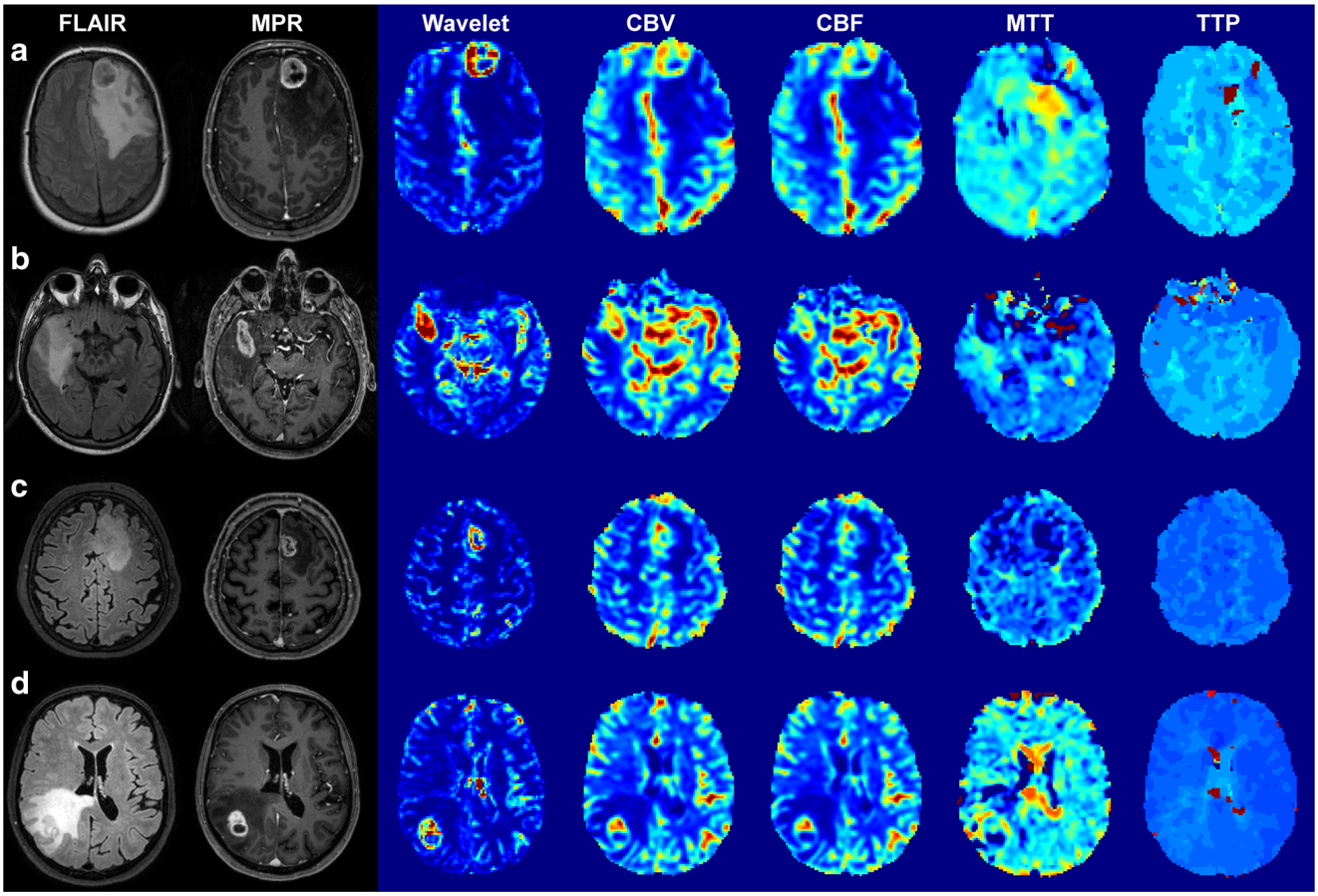

Fig. 3 Exemplary maps of wavelet-MRP. From left to right: FLAIR, T1w MPRAGE, color-coded wavelet-MRP, CBV, BCF, MTT, and TTP in four patients with glioblastoma at the left frontal lobe (**a**), the right temporal lobe (**b**), the left frontal lobe (**c**), and the right parietal lobe (**d**). DSC perfusion data was obtained from a PRESTO sequence (**a**, **b**) and from single-shot gradient-echo EPI protocols (**c**, **d**). Note that highly vascularized tumor tissue shows higher conspicuity compared to surrounding tissue in wavelet-MRP compared to all other conventional DSC maps

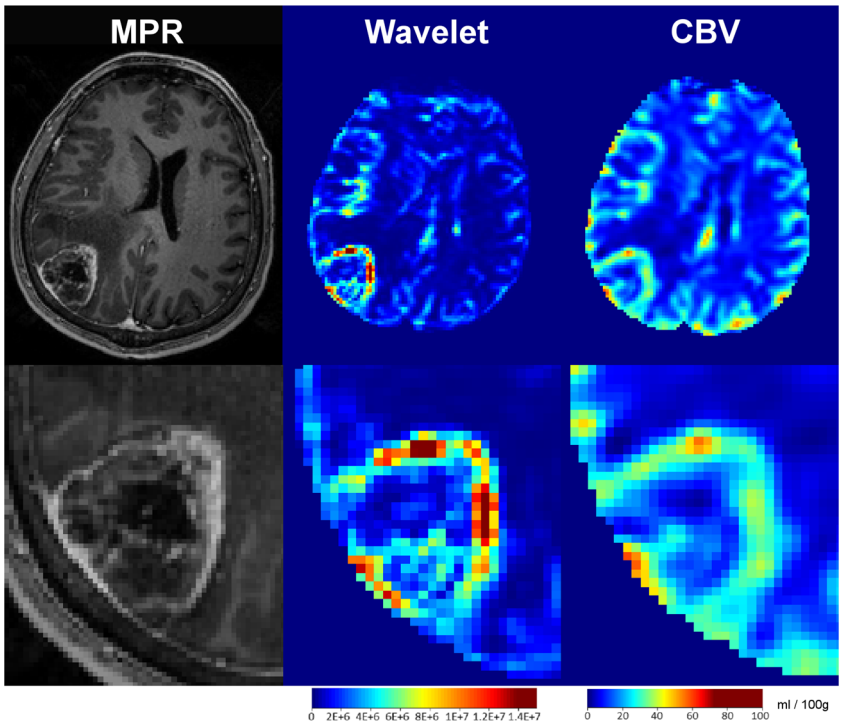

Fig. 4 Improved conspicuity and tumor details in a wavelet-MRP map. The glioblastoma is located at the right parietal lobe in this case. T1-weighted MPRAGE images (**a**), wavelet-MPR (**b**), and CBV maps (**c**) are shown in axial planes. The lower row shows magnified (1:3) details of the tumor. Note that structural features of the contrast-enhancing tumor and its central necrosis are more detailed and in-depth in wavelet-MRP maps. Color-coded CBV values are displayed in ml/100 g; wavelet-MRP parameters are unit free

planning to reduce sampling errors or could be used as a biomarker for response assessment to antiangiogenic therapies [25]. We could further show that wavelet-MRP works robustly with PRESTO and EPI DSC scan protocols.

Relative CBV values have been used for differential diagnosis of glioma and to estimate its grade of malignancy [3, 4]. Wavelet-MRP is of potential interest for further glioma characterization. Moreover, the differentiation between therapy effects and recurrent tumor remains a major challenge in postoperative GBM imaging [7, 8]. Wavelet-MRP might be a powerful additional tool in postoperative PWI due to its high conspicuity and sensitivity for GBM tumor vasculature and vascular hotspots.

As a limitation, the higher discrimination of tumor details in visual image evaluation of wavelet-MRP was similar to the contrast-enhancing structures in T1w MPRAGE images which does not necessarily reflect a true biological correlate. Nevertheless, the overlap between wavelet-MRP and T1 contrast enhancement could be explained by tumor angiogenesis that is often found at the contrast-enhancing border zones of glioblastoma [26]. Further, leakage correction was not performed for wavelet-MRP which might lead to an over- or underestimation of the wavelet signal even though it remains unclear if the leakage effect even disturbs wavelet calculations significantly.

In conclusion, wavelet-MRP is an automated post-processing technique for existing PWI data that yields reproducible perfusion maps with a clear vascular depiction of GBM and potential new clinical applications.

Funding The authors state that this work has not received any specific funding.

Compliance with ethical standards

Guarantor The scientific guarantor of this publication is Dr. Thomas Huber.

Conflict of interest The authors of this manuscript declare relationships with the following companies: TH and LR consultancy for Smart Reporting GmbH (Munich, Germany); BW speaker honoraria from Bayer; TH, JG and SB consultancy for Brainlab AG (Feldkirchen, Germany); JSK research support by DFG, ERC, Acandis—travel support by Kaneka Europe—speaker honoraria by Philips; WHS founder and CEO of Smart Reporting GmbH (Munich, Germany) and founder of Planerio GmbH (Munich, Germany); JR research grant Sirtex Medical Ltd. and research grant Bayer AG; CZ has served on scientific advisory boards for Philips and Bayer Schering; serves as co-editor on the Advisory Board of Clinical Neuroradiology; has received speaker honoraria from Bayer-Schering and Philips and has received research support and investigator fees for clinical studies from Biogen Idec, Quintiles, M.S.D. Sharp & Dome, Boehringer Ingelheim, Inventive Health Clinical U.K. Ltd., Advance Cor, Brainsgate, Pfizer, BayerSchering, Novartis, Roche, Servier, Penumbra, W.C.T. GmbH, Syngis, S.S.S. International Clinical Research, P.P.D. Germany GmbH, Worldwide Clinical Trials Ltd., Phenox, Covidien, Actelion, Medivation, Medtronic, Harrison Clinical Research, Concentric, Penumbra, Pharmtrace, Reverse Medical Corp., Premier Research Germany Ltd., Surpass Medical Ltd., and GlaxoSmithKline. All listed conflicts of interest are unrelated to the present study.

Statistics and biometry One of the authors has significant statistical expertise.

Informed consent Written informed consent was waived by the Institutional Review Board.

Ethical approval Institutional Review Board approval was obtained.

Methodology
- Retrospective
- Experimental
- Performed at one institution

References

1. Guo L, Wang G, Feng Y et al (2016) Diffusion and perfusion weighted magnetic resonance imaging for tumor volume definition in radiotherapy of brain tumors. Radiat Oncol 11:123. https://doi.org/10.1186/s13014-016-0702-y
2. Lee SK (2012) Diffusion tensor and perfusion imaging of brain tumors in high-field MR imaging. Neuroimaging Clin N Am 22:123–134. https://doi.org/10.1016/j.nic.2012.02.001
3. Aronen HJ, Gazit IE, Louis DN et al (1994) Cerebral blood volume maps of gliomas: comparison with tumor grade and histologic findings. Radiology 191:41–51. https://doi.org/10.1148/radiology.191.1.8134596
4. Jain R, Griffith B, Alotaibi F et al (2015) Glioma angiogenesis and perfusion imaging: understanding the relationship between tumor blood volume and leakiness with increasing glioma grade. AJNR Am J Neuroradiol 36:2030–2035. https://doi.org/10.3174/ajnr.A4405
5. Louis DN, Perry A, Reifenberger G et al (2016) The 2016 World Health Organization classification of tumors of the central nervous system: a summary. Acta Neuropathol 131:803–820. https://doi.org/10.1007/s00401-016-1545-1
6. Maeda M, Itoh S, Kimura H et al (1993) Tumor vascularity in the brain: evaluation with dynamic susceptibility-contrast MR imaging. Radiology 189:233–238. https://doi.org/10.1148/radiology.189.1.8372199
7. Hojjati M, Badve C, Garg V et al (2017) Role of FDG-PET/MRI, FDG-PET/CT, and dynamic susceptibility contrast perfusion MRI in differentiating radiation necrosis from tumor recurrence in glioblastomas. J Neuroimaging. https://doi.org/10.1111/jon.12460
8. Chuang MT, Liu YS, Tsai YS, Chen YC, Wang CK (2016) Differentiating radiation-induced necrosis from recurrent brain tumor using MR perfusion and spectroscopy: a meta-analysis. PLoS One 11:e0141438. https://doi.org/10.1371/journal.pone.0141438
9. Singh R, Kesavabhotla K, Kishore SA et al (2016) Dynamic susceptibility contrast-enhanced MR perfusion imaging in assessing recurrent glioblastoma response to superselective intra-arterial bevacizumab therapy. AJNR Am J Neuroradiol 37:1838–1843. https://doi.org/10.3174/ajnr.A4823
10. Ken S, Deviers A, Filleron T et al (2015) Voxel-based evidence of perfusion normalization in glioblastoma patients included in a phase I-II trial of radiotherapy/tipifarnib combination. J Neurooncol 124:465–473. https://doi.org/10.1007/s11060-015-1860-8
11. Kudo K, Christensen S, Sasaki M et al (2013) Accuracy and reliability assessment of CT and MR perfusion analysis software using a digital phantom. Radiology 267:201–211. https://doi.org/10.1148/radiol.12112618
12. Campbell BC, Christensen S, Foster SJ et al (2010) Visual assessment of perfusion-diffusion mismatch is inadequate to select

patients for thrombolysis. Cerebrovasc Dis 29:592–596. https://doi.org/10.1159/000311080
13. Havla L, Thierfelder KM, Beyer SE, Sommer WH, Dietrich O (2015) Wavelet-based calculation of cerebral angiographic data from time-resolved CT perfusion acquisitions. Eur Radiol. https://doi.org/10.1007/s00330-015-3651-1
14. Kunz WG, Schuler F, Sommer WH et al (2017) Wavelet-based angiographic reconstruction of computed tomography perfusion data. Invest Radiol 52:302–309. https://doi.org/10.1097/RLI.0000000000000337
15. Liu G, Sobering G, Duyn J, Moonen CT (1993) A functional MRI technique combining principles of echo-shifting with a train of observations (PRESTO). Magn Reson Med 30:764–768. Available: http://www.ncbi.nlm.nih.gov/pubmed/8139461. Accessed 24 Jul 2018
16. Torrence C, Compo GP (1998) A practical guide to wavelet analysis. Bull Amer Meteor Soc 79:61–78. https://doi.org/10.1175/1520-0477(1998)079<0061:APGTWA>2.0.CO;2
17. Marstal K, Berendsen FF, Staring M, Klein S (2016) SimpleElastix: a user-friendly, multi-lingual library for medical image registration. In: 2016 IEEE Conference on Computer Vision and Pattern Recognition Workshops (CVPRW), Las Vegas, pp 574–582. https://doi.org/10.1109/CVPRW.2016.78
18. Kluge A, Lukas M, Toth V, Pyka T, Zimmer C, Preibisch C (2016) Analysis of three leakage-correction methods for DSC-based measurement of relative cerebral blood volume with respect to heterogeneity in human gliomas. Magn Reson Imaging. https://doi.org/10.1016/j.mri.2015.12.015
19. Yushkevich PA, Piven J, Hazlett HC et al (2006) User-guided 3D active contour segmentation of anatomical structures: significantly improved efficiency and reliability. Neuroimage 31:1116–1128. https://doi.org/10.1016/j.neuroimage.2006.01.015
20. McGraw KO, Wong SP (1996) Forming inferences about some intraclass correlation coefficients. Psychol Methods 30–46. https://doi.org/10.1037/1082-989X.1.1.30
21. Hallgren KA (2012) Computing inter-rater reliability for observational data: an overview and tutorial. Tutor Quant Methods Psychol 8:23–34. https://doi.org/10.1016/j.biotechadv.2011.08.021. Secreted
22. Kelm ZS, Korfiatis PD, Lingineni RK et al (2015) Variability and accuracy of different software packages for dynamic susceptibility contrast magnetic resonance imaging for distinguishing glioblastoma progression from pseudoprogression. J Med Imaging (Bellingham) 2:026001. https://doi.org/10.1117/1.JMI.2.2.026001
23. Hu LS, Kelm Z, Korfiatis P et al (2015) Impact of software modeling on the accuracy of perfusion MRI in glioma. AJNR Am J Neuroradiol 36:2242–2249. https://doi.org/10.3174/ajnr.A4451
24. Korfiatis P, Kline TL, Kelm ZS, Carter RE, Hu LS, Erickson BJ (2016) Dynamic susceptibility contrast-MRI quantification software tool: development and evaluation. Tomography 2:448–456. https://doi.org/10.18383/j.tom.2016.00172
25. Maia AC Jr, Malheiros SM, da Rocha AJ et al (2004) Stereotactic biopsy guidance in adults with supratentorial nonenhancing gliomas: role of perfusion-weighted magnetic resonance imaging. J Neurosurg 101:970–976. https://doi.org/10.3171/jns.2004.101.6.0970
26. Hardee ME, Zagzag D (2012) Mechanisms of glioma-associated neovascularization. Am J Pathol 181:1126–1141. https://doi.org/10.1016/j.ajpath.2012.06.030